

THE RESIDUAL-FREE-BUBBLE FINITE ELEMENT METHOD ON ANISOTROPIC PARTITIONS*

ANDREA CANGIANI[†] AND ENDRE SÜLI[‡]

Abstract. The subject of this work is the analysis and implementation of stabilized finite element methods on anisotropic meshes. We develop the anisotropic a priori error analysis of the residual-free-bubble (RFB) method applied to elliptic convection-dominated convection-diffusion problems in two dimensions, with finite element spaces of type Q_k , $k \geq 1$. In the case of P_1 finite elements, relying on the equivalence of the RFB method to classical stabilized finite element methods, we propose a new rule, justified through the analysis of the RFB method, for selecting the stabilization parameter in classical stabilized methods on two-dimensional anisotropic triangulations.

Key words. residual-free-bubble finite element method, convection-dominated diffusion problems, stabilized finite element methods

AMS subject classifications. 65N12, 65N39, 76M10

DOI. 10.1137/060658011

1. Introduction. Elliptic convection-diffusion problems arise in a vast number of applications, and their stable, accurate, and efficient solution is of significant theoretical and practical interest. From the computational point of view, problems of this kind become particularly challenging when convection dominates diffusion in the sense that the Péclet number, which measures the magnitude of the convective vector field over the length scale of the computational domain relative to the size of the diffusion coefficient, is large. Convection-dominated diffusion equations exhibit features which resemble those of the *reduced*, first-order hyperbolic equation arising from the second-order elliptic convection-diffusion equation on neglecting the diffusion term. For example, the solution may contain thin internal layers within the computational domain; also, due to the singular perturbation nature of an elliptic convection-dominated diffusion problem, the solution may exhibit thin boundary layers along sections of the boundary of the computational domain which correspond to the outflow part of the boundary for the reduced problem. As a result of this, on meshes which do not resolve internal and boundary layers, standard Galerkin finite element methods have poor stability and accuracy properties. The difficulties typically manifest themselves as large, maximum-principle-violating, oscillations in the numerical solution which occur predominantly along the characteristics of the reduced problem.

The situation may be remedied by using a classical stabilized finite element method (such as a streamline-diffusion method or a Galerkin least-squares method) or a residual-free-bubble (RFB) finite element method; we refer to the monograph [28] for an extensive survey of the literature. Due to the presence of anisotropic numerical dissipation terms in the direction of the characteristics of the reduced equation whose role is to suppress undesirable numerical oscillations, these methods are capable of delivering accurate numerical solutions even on shape-regular computational meshes

*Received by the editors April 24, 2006; accepted for publication (in revised form) May 9, 2007; published electronically August 17, 2007.

<http://www.siam.org/journals/sinum/45-4/65801.html>

[†]Dipartimento di Matematica, Università di Pavia, 27000 Pavia, Italy (andrea.cangiani@unipv.it).

[‡]Numerical Analysis Group, Oxford University Computing Laboratory, Oxford OX1 3QD, England (endre.suli@comlab.ox.ac.uk).

whose granularity is relatively coarse compared to the thickness of internal and boundary layers. Alternatively, motivated by the fact that internal and boundary layers are highly localized and anisotropic, one may choose to use a standard Galerkin finite element method, albeit on a stretched, anisotropic, or layer-adapted (and, certainly, non-shape-regular) computational mesh (see, for example, the discussion in [28] on Shishkin-type meshes).

In recent years, there have been attempts to employ these remedies simultaneously; see, for example, the work of Apel and Lube [3] and Micheletti, Perotto, and Picasso [25] concerning classical stabilized finite element methods on anisotropic meshes. The developments in the present article are in a similar spirit.

The objective of this paper is twofold. We aim to develop the a priori error analysis of the RFB method for two-dimensional elliptic convection-dominated diffusion equations on anisotropic partitions. Specifically, we aim to bound the error by appropriately weighted norms of directional derivatives of the solution, so as to incorporate the anisotropic nature of the solution into the bounds. On the one hand, our results complement the work in [3, 25] on the a priori error analysis of classical stabilized finite element methods over anisotropic meshes; on the other hand, they extend earlier results by Brezzi, Marini, and Süli [7], Brezzi and Marini [8], and Sangalli [29] on the a priori error analysis of RFB methods on shape-regular triangulations.

Anisotropy also has to be taken into account in the selection of parameters appearing in stabilized finite element methods, such as *streamline-diffusion-type* methods. The second key objective of the paper is to use the stabilizing term derived from the RFB method to redefine the mesh Péclet number and propose a new choice of the streamline-diffusion (SD) parameter that is suitable for use on anisotropic partitions. The proposed choice of the SD parameter improves earlier suggestions based on the a priori analysis of the streamline-diffusion method (cf. [3, 23, 25]).

The paper is structured as follows. The first part of this work is concerned with the analysis of stabilized finite element methods on anisotropic computational meshes: We consider the anisotropic a priori error analysis of the RFB method applied to elliptic convection-dominated convection-diffusion problems in two dimensions. In the second part of the paper, in the case of P_1 finite elements on triangular meshes, appealing to the equivalence of the RFB method to classical stabilized finite element methods, we propose a new rule, justified through the analysis of the RFB method, for selecting the stabilization parameter in classical stabilized methods on two-dimensional anisotropic triangulations; we then relate our work to existing developments on classical stabilized finite element methods on anisotropic meshes, including [3, 23, 25].

2. Statement of the problem. Let $\Omega \subset \mathbb{R}^2$ be a bounded open polygonal domain. We consider the model elliptic boundary-value problem

$$(2.1) \quad \begin{cases} \text{find } u \in V = H_0^1(\Omega) \text{ such that} \\ Lu := -\varepsilon \Delta u + \mathbf{a} \cdot \nabla u = f \quad \text{in } \Omega, \end{cases}$$

where ε is a positive parameter, $\mathbf{a} \in [W^{1,\infty}(\Omega)]^2$, with $\text{div}(\mathbf{a}) \leq 0$ in Ω , and f belongs to $L^2(\Omega)$. The homogeneous Dirichlet boundary condition $u|_{\partial\Omega} = 0$ has been assumed here only for ease of presentation. We normalize the problem by requiring that $\|\mathbf{a}\|_{L^\infty(\Omega)} \leq 1$. Our focus of interest is the convection-dominated regime, namely, when $0 < \varepsilon \ll 1$; thus we assume, without loss of generality, that $\varepsilon \in (0, 1]$. The extension of the results of this paper to the, more general, convection-diffusion-reaction equation $-\varepsilon \Delta u + \mathbf{a} \cdot \nabla u + cu = f$ in Ω , subject to a homogeneous Dirichlet boundary

condition on $\partial\Omega$, is straightforward, provided that $\operatorname{div}(\mathbf{a}) - 2c \leq 0$ in Ω . Below, we shall briefly comment on the case when $\operatorname{div}(\mathbf{a}) - 2c \leq -2c_0$ in Ω , where c_0 is a positive constant.

The variational formulation of the boundary-value problem (2.1) is

$$(2.2) \quad \begin{cases} \text{find } u \in V \text{ such that} \\ \mathcal{L}(u, v) = (f, v) \quad \forall v \in V, \end{cases}$$

where

$$(2.3) \quad \mathcal{L}(w, v) := \varepsilon \int_{\Omega} \nabla w \cdot \nabla v \, d\mathbf{x} + \int_{\Omega} (\mathbf{a} \cdot \nabla w) v \, d\mathbf{x}$$

is a continuous and coercive bilinear form on $V \times V$ and (\cdot, \cdot) denotes the L^2 inner product over Ω .

The existence and uniqueness of a solution to (2.2) (that is, of a weak solution to (2.1)) are well-known consequences of the Lax–Milgram lemma; for a more general existence and uniqueness result, see [19, Theorem 8.6].

We consider finite element discretizations of (2.2) over *conforming* partitions \mathcal{T}_h of $\bar{\Omega}$ consisting of affine-equivalent quadrilateral or triangular elements. We shall not assume that the family of partitions $\{\mathcal{T}_h\}_{h>0}$ is *shape-regular*, because we wish to allow anisotropic local refinements in parts of the computational domain where special features of the exact solution, such as thin layers, are detected. Our only assumption will be the existence of a positive constant $c \leq 1$ such that

$$(2.4) \quad \varepsilon \leq ch_{\gamma},$$

for all element edges γ in the partition; here h_{γ} represents the length of γ . This is a reasonable assumption when dealing with the analysis of stabilized finite element methods for convection-dominated diffusion problems such as our model problem, which exhibits boundary layers whose thickness is commensurate with $\varepsilon \ll 1$: For, if we could afford to solve the problem on meshes whose granularity is smaller than ε , then we would not need to use a stabilized method in the first place. Thus, our a priori error bounds, developed under the hypothesis (2.4), will be of a *preasymptotic* nature: Since the lower bound $\varepsilon \ll 1$ on ch_{γ} is fixed, we will *not* let h_{γ} tend to zero.

An optimal mesh (in terms of the number of degrees of freedom required to obtain a given accuracy) must mimic the behavior of the solution to (2.1). Such an optimal mesh would, in general, be designed through successive mesh refinements/de-refinements. In early stages of the mesh adaptation process, the use of a stabilized finite element method is mandatory, since on coarse meshes classical Galerkin finite element approximations of (2.1) will exhibit large maximum-principle-violating numerical oscillations when $\varepsilon \ll 1$, hence the need for sharp preasymptotic error bounds for stabilized finite element methods. In later stages of the mesh refinement process, when the mesh has been adapted to the solution, the stabilized method could be simplified, for instance, by omitting the stabilization term, as was done in [10].

We denote by λ_1 and λ_2 some characteristic dimensions of a generic element $T \in \mathcal{T}_h$, to be defined on a case-by-case basis; λ_1 and λ_2 are used to group the elements according to the following rule (which defines the subpartitions \mathcal{T}_1 and \mathcal{T}_2):

1. $T \in \mathcal{T}_1$ if $\lambda_1 \leq \lambda_2$;
2. $T \in \mathcal{T}_2$ if $\lambda_2 < \lambda_1$.

An admissible structured mesh and its subpartitions are shown in Figure 2.1.

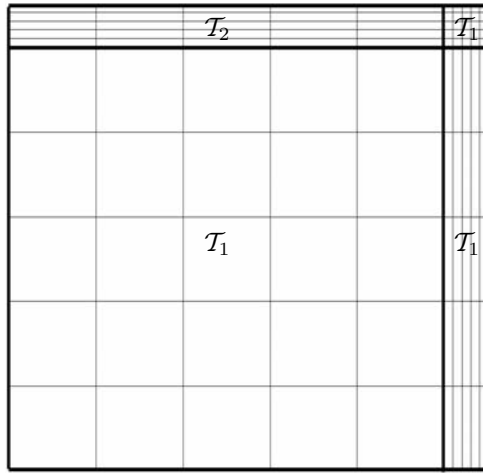


FIG. 2.1. A locally anisotropic partition and its subpartitions \mathcal{T}_1 and \mathcal{T}_2 .

Given $k \geq 1$, let \mathcal{P}_k denote the space of algebraic polynomials of degree $\leq k$, and let \mathcal{Q}_k denote the space of algebraic polynomials of degree $\leq k$ with respect to each variable. Further, let $F_T : \hat{T} \rightarrow T$ be the affine transformation mapping the reference element onto $T \in \mathcal{T}_h$.

The residual-free-bubble space is defined as follows (see [7]):

$$(2.5) \quad V_{\text{RFB}} := \{v \in V : v|_e \in \mathcal{P}_k \text{ for each edge } e \text{ of } T \text{ and any element } T \in \mathcal{T}_h\}.$$

We note that the space V_{RFB} is infinite-dimensional, admitting the representation

$$(2.6) \quad V_{\text{RFB}} = V_h^k + B_h,$$

where V_h^k is the classical finite element space given by

$$V_h^k := \left\{ v_h \in H_0^1(\Omega) : \begin{cases} v_h|_T \in \mathcal{P}_k & \text{if } T \text{ is a triangle} \\ v_h|_T \circ F_T \in \mathcal{Q}_k & \text{if } T \text{ is a parallelogram} \end{cases} \right\},$$

and

$$(2.7) \quad B_h := \bigoplus_{T \in \mathcal{T}_h} H_0^1(T)$$

is the space of all bubble functions in V ; i.e., all function with zero trace on the skeleton of the partition \mathcal{T}_h .

The RFB approximation of (2.2) is defined as the Galerkin approximation of (2.2) in the space V_{RFB} :

$$(2.8) \quad \begin{cases} \text{find } u_{\text{RFB}} \in V_{\text{RFB}} \text{ such that} \\ \mathcal{L}(u_{\text{RFB}}, v) = (f, v) \quad \forall v \in V_{\text{RFB}}. \end{cases}$$

Since V_{RFB} is infinite-dimensional, the formulation (2.8) does not represent a numerical method in the classical sense. In fact, a numerical algorithm can be devised from (2.8) through static condensation of the bubble component u_b of the solution u_{RFB} ,

which belongs to the infinite-dimensional space B_h , and then discretizing the resulting infinite-dimensional problem over the finite-dimensional space V_h^k . For instance, if $k \leq 2$, the sum in (2.7) is direct, and hence we then have the following unique decomposition of the RFB solution:

$$u_{\text{RFB}} = u_h + u_b.$$

Consequently, by testing in V_h^k and then in B_h , we can split (2.8) into the following two problems:

$$(2.9) \quad \mathcal{L}(u_h, v_h) + \mathcal{L}(u_b, v_h) = (f, v_h) \quad \forall v_h \in V_h^k,$$

$$(2.10) \quad \mathcal{L}(u_h, v_b) + \mathcal{L}(u_b, v_b) = (f, v_b) \quad \forall v_b \in B_h.$$

Equation (2.10) is referred to as a *bubble equation* as it is equivalent to solving, in each element $T \in \mathcal{T}_h$, the boundary-value problem

$$(2.11) \quad \begin{cases} Lu_b = f - Lu_h & \text{in } T, \\ u_b = 0 & \text{on } \partial T \end{cases}$$

for the “fine-scale” bubble component u_b of the approximate solution u_{RFB} in terms of the “coarse-scale” piecewise polynomial component u_h of u_{RFB} . The static condensation procedure corresponds to eliminating u_b from (2.9) in favor of u_h using (2.11). This can be done by numerically solving a finite number of independent local problems such as (2.11); this then leads to a (fully discrete) numerical algorithm. An instance of such a procedure is discussed in section 6 of this paper. For further details, we refer the reader to [9, 7].

The general a priori error analysis of the RFB method on shape-regular partitions is due to Brezzi, Marini, and Süli [7]; it was shown there that if $u \in H^{k+1}(\Omega)$, then the numerical solution u_{RFB} delivered by the RFB method satisfies the following optimal asymptotic error bound in the energy norm:

$$(2.12) \quad \varepsilon^{1/2} |u - u_{\text{RFB}}|_{1,\Omega} \leq Ch^{k+1/2} \|u\|_{H^{k+1}(\Omega)},$$

where h represents the characteristic size of the partition.

The technique used here to extend the a priori error analysis of the RFB method to anisotropic partitions is different from the one employed in [7]. Instead, we follow the approach adopted by Sangalli [29] to subsequently rederive and localize the results presented in [7]. The key idea of Sangalli’s approach, and of the analysis below, is to exploit the approximation properties of the space V_{RFB} . To do so, Sangalli explicitly constructs a projector from H^1 onto the RFB space in a certain ε -weighted H^1 norm. A similar approach is followed by Risch in [27].

A second key ingredient of our analysis is the use of anisotropic approximation results. These must be employed in order to derive an a priori error bound in terms of appropriately weighted norms of directional derivatives of the exact solution u .

3. Structured quadrilateral partitions. We begin with the case of axiparallel rectangular elements, leaving the treatment of more general partitions to subsequent sections.

In this case it is natural to define $\lambda_1 = h_1$ and $\lambda_2 = h_2$, where h_1 and h_2 denote the dimensions of the generic element $T \in \mathcal{T}$ in the x_1 and x_2 coordinate directions, respectively.

3.1. Notations and preliminary results. Let $\widehat{T} = (-1, 1)^2$ be the master element. Given a function $v \in H^1(T)$, we consider $\widehat{v} \in H^1(\widehat{T})$, the function associated to v through the affine transformation F_T which maps \widehat{T} into T ; hence $\widehat{v} := v \circ F_T$. Further, we denote by $i^* = 3 - i$ the complementary index to i with respect to the set $\{1, 2\}$.

Since T is a rectangle, the usual scaling properties for functions $v \in H^1(T)$ yield

$$(3.1) \quad \|v\|_{0,T}^2 = \frac{1}{4} h_1 h_2 \|\widehat{v}\|_{0,\widehat{T}}^2,$$

$$(3.2) \quad \left\| \frac{\partial v}{\partial x_i} \right\|_{0,T}^2 = \frac{h_{i^*}}{h_i} \left\| \frac{\partial \widehat{v}}{\partial \widehat{x}_i} \right\|_{0,\widehat{T}}^2, \quad i \in \{1, 2\}.$$

We will also need some scaling properties for functions defined over edges of the elements $T \in \mathcal{T}_h$. The trace of a function belonging to the space $H^1(T) = W^{1,2}(T)$ and, more generally, to the Sobolev space $W^{1,p}(T)$, $1 \leq p < \infty$, is characterized in terms of the *fractional-order* Sobolev space $W^{1-1/p,p}(\partial T)$, which, for $p > 1$, can be defined using the real method of function space interpolation; see, e.g., Adams [1].

The space $W^{s,p}(\partial T)$, $0 < s < 1$, can also be characterized in terms of an intrinsically defined norm. For instance, for every $s \in (0, 1)$, the norm $\|\cdot\|_{s,\partial T}$ and seminorm $|\cdot|_{s,\partial T}$ of the Sobolev space $H^s(\partial T) = W^{s,2}(\partial T)$ of fractional order s are defined by

$$(3.3) \quad \begin{aligned} \|v\|_{s,\partial T} &:= \left\{ \|v\|_{0,\partial T}^2 + \int_{\partial T} \int_{\partial T} \frac{|v(\mathbf{x}) - v(\mathbf{y})|^2}{|\mathbf{x} - \mathbf{y}|^{1+2s}} d\sigma(\mathbf{x}) d\sigma(\mathbf{y}) \right\}^{1/2} \\ &= \{ \|v\|_{0,\partial T}^2 + |v|_{s,\partial T}^2 \}^{1/2}, \end{aligned}$$

where $d\sigma$ denotes the one-dimensional Hausdorff measure of ∂T . This definition can be extended to portions of ∂T .

The trace theorem (again, see [1]) ensures that the trace of a function $v \in H^s(T)$ belongs to $H^{s-1/2}(\partial T)$, $s \in (1/2, 1]$, and that there exists a constant C , independent of v , such that

$$(3.4) \quad \|v\|_{s-1/2,\partial T} \leq C \|v\|_{s,T} \quad \forall v \in H^s(T).$$

Let γ be an edge of $T \in \mathcal{T}_h$ and $\widehat{\gamma} = F_T^{-1}(\gamma)$ the corresponding edge of \widehat{T} . Scaling the Sobolev seminorm $|\cdot|_{s,\gamma}$, $0 \leq s \leq 1$, from $\widehat{\gamma}$ to γ , we have

$$(3.5) \quad |v|_{s,\gamma}^2 = \left(\frac{h_\gamma}{2} \right)^{1-2s} |\widehat{v}|_{s,\widehat{\gamma}}^2 \quad \forall v \in H^s(\gamma),$$

where, as before, $h_\gamma = |\gamma|$. The scaling property (3.5) will be used to prove the following anisotropic trace inequalities which are refinements of the usual ones valid for axiparallel domains.

LEMMA 3.1. *Let $v \in H^1(T)$, where T is an axiparallel rectangle in \mathbb{R}^2 , and let γ_i be an edge of T parallel to the i th coordinate axis, with $h_i = |\gamma_i|$, $i = 1, 2$. The following trace inequalities hold:*

$$(3.6) \quad \|v\|_{0,\gamma_i}^2 \leq \frac{1}{h_{i^*}} \|v\|_{0,T}^2 + 2 \|v\|_{0,T} \|v_{x_{i^*}}\|_{0,T}, \quad i = 1, 2;$$

$$(3.7) \quad |v|_{1/2,\partial T}^2 \leq C \left(\frac{1}{h_1 h_2} \|v\|_{0,T}^2 + \frac{h_1}{h_2} \|v_{x_1}\|_{0,T}^2 + \frac{h_2}{h_1} \|v_{x_2}\|_{0,T}^2 \right),$$

where the constant C is independent of h_1 and h_2 .

Proof. The proof of (3.6) can be found, for instance, in [17]. To prove (3.7), we apply (3.5) with $s = 1/2$ to scale from ∂T to $\partial \widehat{T}$ and the trace inequality (3.4) to shift from $\partial \widehat{T}$ to \widehat{T} , and, finally, we use (3.1) and (3.2) to scale back from \widehat{T} to T :

$$\begin{aligned} |v|_{1/2, \partial T}^2 &= |\hat{v}|_{1/2, \partial \widehat{T}}^2 \leq \|\hat{v}\|_{1/2, \partial \widehat{T}}^2 \leq C \|\hat{v}\|_{1, \widehat{T}}^2 \\ &= C \left(\|\hat{v}\|_{0, \widehat{T}}^2 + \|\hat{v}_{x_1}\|_{0, \widehat{T}}^2 + \|\hat{v}_{x_2}\|_{0, \widehat{T}}^2 \right) \\ &= C \left(\frac{1}{h_1 h_2} \|v\|_{0, T}^2 + \frac{h_1}{h_2} \|v_{x_1}\|_{0, T}^2 + \frac{h_2}{h_1} \|v_{x_2}\|_{0, T}^2 \right) \end{aligned}$$

and hence the desired result for any $v \in H^1(T)$. \square

We shall also require the following trace-lifting lemma (see, e.g., Sangalli [29]).

LEMMA 3.2. *Given a function $\hat{w}_0 \in H^{1/2}(\partial \widehat{T})$ and a real parameter t , with $0 < t \leq 1$, there exists $\hat{w} \in H^1(\widehat{T})$ such that $\hat{w} = \hat{w}_0$ on $\partial \widehat{T}$ and*

$$(3.8) \quad t |\hat{w}|_{1, \widehat{T}}^2 + t^{-1} \|\hat{w}\|_{0, \widehat{T}}^2 \leq C \left(t |\hat{w}_0|_{1/2, \partial \widehat{T}}^2 + \|\hat{w}_0\|_{0, \partial \widehat{T}}^2 \right),$$

where the constant C is independent of t and \hat{w}_0 .

3.2. The projection error. Let us consider the function space $H^{r_1, r_2}(T)$ of dominant mixed smoothness, defined by

$$H^{r_1, r_2}(T) := \{v \in L^2(T) : D_{x_1}^{r_1} v, D_{x_2}^{r_2} v, D_{x_1}^{r_1} D_{x_2}^{r_2} v \in L^2(T)\}.$$

It is known that if $r_i > 1/2$, $i = 1, 2$, then $H^{r_1, r_2}(T)$ is continuously embedded into the space $C(\overline{T})$ of uniformly continuous functions on \overline{T} (see, for example, [32, Chapter 2, Theorem 2.2.3]). Trivially, $H^{r+1}(T)$ is continuously embedded into $H^{1,1}(T)$ for any $r \geq 1$.

We begin by introducing a suitable interpolant from \mathcal{Q}_k of a generic function in $H^{1,1}(T)$ — the tensor-product H^1 -projection operator Π_k , as has been defined in [17] (see also [31, 18]), by means of truncated Legendre expansions.

DEFINITION 3.3. *Let L_n denote the Legendre polynomial of degree n on the open interval $I = (-1, 1)$. We define the L^2 -projection operator*

$$\tilde{\pi}_k : L^2(I) \rightarrow \mathcal{P}_k(I)$$

by

$$\tilde{\pi}_k v(x) := \sum_{n=0}^k a_n L_n(x),$$

where

$$a_n := \frac{2n+1}{2} \int_I v(x) L_n(x) dx.$$

Further, we define the H^1 -projection operator

$$\hat{\pi}_k : H^1(I) \rightarrow \mathcal{P}_k(I)$$

by setting, for any $v \in H^1(I)$,

$$\hat{\pi}_k v(x) := \int_{-1}^x \tilde{\pi}_{k-1}(v')(\eta) d\eta + v(-1), \quad x \in (-1, 1).$$

A convenient feature of the above definition is that it can be easily extended to the multidimensional setting by means of a tensor-product construction; this is achieved at the cost of assuming additional regularity (viz. assuming $H^{1,1}$ -regularity instead of H^1 -regularity).

DEFINITION 3.4. Let $\widehat{T} = (-1, 1)^2$. We define the tensor-product projection operator

$$\widehat{\Pi}_k : H^{1,1}(\widehat{T}) \rightarrow \mathcal{Q}_k(\widehat{T})$$

by

$$\widehat{\Pi}_k := \widehat{\pi}_k^{x_1} \circ \widehat{\pi}_k^{x_2},$$

where $\widehat{\pi}_k^{x_1}, \widehat{\pi}_k^{x_2}$ denote the one-dimensional H^1 -projection operators from Definition 3.3, and the superscripts $x_i, i = 1, 2$, indicate the directions in which the one-dimensional projections are applied.

The above definition is easily extended to a generic axiparallel rectangle T as follows.

DEFINITION 3.5. Let $T \in \mathcal{T}_h$. We define the tensor-product projection operator

$$\Pi_k : H^{1,1}(T) \rightarrow \mathcal{Q}_k(T)$$

by setting, for any $v \in H^{1,1}(T)$,

$$\Pi_k v := \widehat{\Pi}_k \widehat{v} \circ F_T^{-1}.$$

By virtue of being of tensor-product type, the projection Π_k admits anisotropic error bounds. As a matter of fact, it is better-behaved than the L^2 -projection operator when bounds on the derivatives of the interpolation error are needed. The relevant approximation properties of Π_k are summarized in the next lemma.

LEMMA 3.6. Suppose that T is an axiparallel rectangle and $v \in H^{r+1}(T)$, with $1 \leq r \leq k$ —and thereby $v \in H^{1,1}(T)$. Then, for any s with $0 \leq s \leq r$, the following error bound holds:

$$\begin{aligned} \|v - \Pi_k v\|_{0,T}^2 &\leq \Phi_2(k, s) \left(\left(\frac{h_1}{2}\right)^{2s+2} \|\partial_{x_1}^{s+1} v\|_{0,T}^2 + \left(\frac{h_2}{2}\right)^{2s+2} \|\partial_{x_2}^{s+1} v\|_{0,T}^2 \right) \\ &\quad + \Phi_2(k, s - 1) \min_{\substack{i, j = 1, 2 \\ i \neq j}} \left(\frac{h_i}{2}\right)^2 \left(\frac{h_j}{2}\right)^{2s} \|\partial_{x_j}^s \partial_{x_i} v\|_{0,T}^2, \end{aligned}$$

and, for any $i = 1, 2$,

$$\|\partial_{x_i}(v - \Pi_k v)\|_{0,T}^2 \leq \Phi_1(k, s) \left(\frac{h_i}{2}\right)^{2s} \|\partial_{x_i}^{s+1} v\|_{0,T}^2 + \Phi_2(k, s - 1) \left(\frac{h_{i^*}}{2}\right)^{2s} \|\partial_{x_{i^*}}^s \partial_{x_i} v\|_{0,T}^2,$$

where

$$\Phi_1(k, s) := \left(\frac{\Gamma(k - s + 1)}{\Gamma(k + s + 1)}\right)^{1/2}, \quad \Phi_2(k, s) := \frac{\Phi_1(k, s)}{\sqrt{k(k + 1)}},$$

and Γ is the Gamma function.

The proof of the interpolation error bounds stated in the above lemma has been given by Georgoulis in [17] (see also [18]), where such results are presented in a much more general setting.

Remark. Interpolation error bounds similar to those in Lemma 3.6 are provided, although for a different interpolation operator, by Apel [2, Theorem 2.7]. These, too, are limited to rectangular elements and are obtained as improvements of the general but slightly less sharp bounds presented in earlier sections of [2]; see also section 4 (especially Theorem 4.10) in the recent work of Georgoulis, Hall, and Houston [16] concerning interpolation results on anisotropic nonaxiparallel meshes. For a recent survey of anisotropic mesh adaptivity and anisotropic interpolation error estimates, particularly on triangular meshes, we refer to the work of Huang [21].

3.3. Error bound. Suppose that the bounded polygonal domain $\Omega \subset \mathbb{R}^2$ is a finite union of axiparallel rectangles. We begin the error analysis with the construction of a suitable projector $P : H_0^1(\Omega) \cap H^2(\Omega) \rightarrow V_{\text{RFB}}$, whose definition is based on the $H^{1,1}$ -projection operator Π_k described above and the trace-lifting lemma, Lemma 3.2.

Given $\hat{v} \in H^{1,1}(\hat{T}) \subset H^1(\hat{T})$, let $\hat{w} \in H^1(\hat{T})$ be the function obtained by applying Lemma 3.2 with

$$\hat{w}_0 = (\hat{v} - \hat{\Pi}_k \hat{v})|_{\partial \hat{T}}, \quad t = \frac{\varepsilon}{h_i}.$$

We note that $t \leq 1$ due to assumption (2.4). We define $P_{\hat{T}} \hat{v} \in H^1(\hat{T})$ by

$$(3.9) \quad P_{\hat{T}} \hat{v} := \hat{v} - \hat{w},$$

and let $P_T v = P_{\hat{T}} \hat{v} \circ F_T^{-1}$. Finally, for $v \in H_0^1(\Omega) \cap H^2(\Omega)$, we define $Pv \in H_0^1(\Omega)$ elementwise by $(Pv)|_T = P_T(v|_T)$, $T \in \mathcal{T}_h$; recall that $v|_T \in H^2(T) \subset H^{1,1}(T)$, so this definition is meaningful. It is clear from this construction that, for every element $T \in \mathcal{T}_h$, $P_T : H^{1,1}(T) \rightarrow V_{\text{RFB}}|_T$, and $P : H_0^1(\Omega) \cap H^2(\Omega) \rightarrow V_{\text{RFB}}$.

The main task in the a priori error analysis is to bound the quantity $\mathcal{E}_T^P(v)$ defined for $v \in H^{1,1}(T)$ by

$$(3.10) \quad \mathcal{E}_T^P(v) := \varepsilon |v - P_T v|_{1,T}^2 + \varepsilon^{-1} \|v - P_T v\|_{0,T}^2.$$

To this end, let us assume that $T \in \mathcal{T}_i$, with $i \in \{1, 2\}$. Using (3.1) and (3.2), and noting that for $T \in \mathcal{T}_i$ we have $h_i \leq h_{i^*}$, it follows that

$$(3.11) \quad \begin{aligned} \mathcal{E}_T^P(v) &= \varepsilon \frac{h_i}{h_{i^*}} \|(\hat{v} - P_{\hat{T}} \hat{v})_{\hat{x}_{i^*}}\|_{0,\hat{T}}^2 + \varepsilon \frac{h_{i^*}}{h_i} \|(\hat{v} - P_{\hat{T}} \hat{v})_{\hat{x}_i}\|_{0,\hat{T}}^2 + \frac{\varepsilon^{-1} h_{i^*} h_i}{4} \|\hat{v} - P_{\hat{T}} \hat{v}\|_{0,\hat{T}}^2 \\ &\leq Ch_{i^*} \left(\frac{\varepsilon}{h_i} |\hat{v} - P_{\hat{T}} \hat{v}|_{1,\hat{T}}^2 + \left(\frac{\varepsilon}{h_i} \right)^{-1} \|\hat{v} - P_{\hat{T}} \hat{v}\|_{0,\hat{T}}^2 \right). \end{aligned}$$

Hence, by applying (3.8) in (3.11) with $\hat{w} = \hat{v} - P_{\hat{T}} \hat{v}$, we have

$$(3.12) \quad \mathcal{E}_T^P(v) \leq C \left(\varepsilon \frac{h_{i^*}}{h_i} |\hat{v} - \hat{\Pi}_k \hat{v}|_{1/2,\partial \hat{T}}^2 + h_{i^*} \|\hat{v} - \hat{\Pi}_k \hat{v}\|_{0,\partial \hat{T}}^2 \right).$$

We are now in a position to prove the following result which justifies our choice of the projector P .

LEMMA 3.7. *Let $T \in \mathcal{T}$ and $v \in H^{r+1}(T)$, with $1 \leq r \leq k$, and consider the quantity $\mathcal{E}_T^P(v)$ defined by (3.10). If $T \in \mathcal{T}_i$, $i \in \{1, 2\}$, then*

$$(3.13) \quad \begin{aligned} \mathcal{E}_T^P(v) \leq & \frac{C}{2^{2r+1}} \left(\Phi_{12}(k, r) \left(h_i^{2r+1} \|\partial_{x_i}^{r+1} v\|_{0,T}^2 + \frac{h_{i^*}^{2r+2}}{h_i} \|\partial_{x_{i^*}}^{r+1} v\|_{0,T}^2 \right) \right. \\ & \left. + \frac{5}{2} \Phi_2(k, r-1) (h_i^{2r-1} h_{i^*}^2 \|\partial_{x_i}^r \partial_{x_{i^*}} v\|_{0,T}^2 + h_i h_{i^*}^{2r} \|\partial_{x_i} \partial_{x_{i^*}}^r v\|_{0,T}^2) \right), \end{aligned}$$

where $\Phi_{12}(k, r) := 2\Phi_1(k, r) + \Phi_2(k, r)/2$.

Proof. Assume that $T \in \mathcal{T}_i$, $i \in \{1, 2\}$, and let $\partial_{x_i} T$ and $\partial_{x_{i^*}} T$ be the collection of the edges of T parallel to the x_i and x_{i^*} coordinate directions, respectively. From (3.12), upon returning to ∂T using (3.5) and applying the trace inequalities of Lemma 3.1, we have

$$\begin{aligned} \mathcal{E}_T^P(v) & \leq C \left(\varepsilon \frac{h_{i^*}}{h_i} \|v - \Pi_k v\|_{1/2, \partial T}^2 + 4 \|v - \Pi_k v\|_{0, \partial_{x_{i^*}} T}^2 + 4 \frac{h_{i^*}}{h_i} \|v - \Pi_k v\|_{0, \partial_{x_i} T}^2 \right) \\ & \leq C \left(\left(\frac{\varepsilon}{h_i^2} + \frac{1}{h_i} \right) \|v - \Pi_k v\|_{0,T}^2 + \varepsilon \frac{h_{i^*}^2}{h_i^2} \|(v - \Pi_k v)_{x_{i^*}}\|_{0,T}^2 + \varepsilon \|(v - \Pi_k v)_{x_i}\|_{0,T}^2 \right. \\ & \quad \left. + \frac{h_{i^*}}{h_i} \|v - \Pi_k v\|_{0,T} \|(v - \Pi_k v)_{x_{i^*}}\|_{0,T} + \|v - \Pi_k v\|_{0,T} \|(v - \Pi_k v)_{x_i}\|_{0,T} \right) \\ & \leq C \left(\left(\frac{\varepsilon}{h_i^2} + \frac{1}{h_i} \right) \|v - \Pi_k v\|_{0,T}^2 \right. \\ & \quad \left. + \left(\varepsilon \frac{h_{i^*}^2}{h_i^2} + \frac{h_{i^*}^2}{h_i} \right) \|(v - \Pi_k v)_{x_{i^*}}\|_{0,T}^2 + (\varepsilon + h_i) \|(v - \Pi_k v)_{x_i}\|_{0,T}^2 \right). \end{aligned}$$

With assumption (2.4) this bound may be written

$$\mathcal{E}_T^P(v) \leq C \left(\frac{1}{h_i} \|v - \Pi_k v\|_{0,T}^2 + \frac{h_{i^*}^2}{h_i} \|(v - \Pi_k v)_{x_{i^*}}\|_{0,T}^2 + h_i \|(v - \Pi_k v)_{x_i}\|_{0,T}^2 \right).$$

Thus, we have bounded $\mathcal{E}_T^P(v)$ in terms of the H^1 -projection error. The required bound (3.13) follows by applying the projection error bounds from Lemma 3.6. \square

We are ready to prove the following a priori error bound for the RFB method in the energy norm $\varepsilon^{1/2} |\cdot|_{1,\Omega}$.

THEOREM 3.8. *Let $u \in V$ be the solution of (2.2) and $u_{\text{RFB}} \in V_{\text{RFB}}$ the RFB solution defined by (2.8). Assume that the partition \mathcal{T}_h consists of axiparallel rectangles and that there exists a constant $c \in (0, 1]$ such that, for any $T \in \mathcal{T}_h$, $\varepsilon \leq c \min\{h_1, h_2\}$. Finally, let \mathcal{T}_1 be the subpartition given by all $T \in \mathcal{T}_h$ such that $h_1 \leq h_2$, and let $\mathcal{T}_2 := \mathcal{T}_h \setminus \mathcal{T}_1$.*

If $u \in H_0^1(\Omega) \cap H^{k+1}(\Omega)$, then there exists a positive constant C , independent of ε , k and of the mesh dimensions, such that for any $1 \leq r \leq k$

$$(3.14) \quad \begin{aligned} \varepsilon^{1/2} |u - u_{\text{RFB}}|_{1,\Omega} \leq & C \frac{\bar{\Phi}(k, r)}{2^{r+1/2}} \sum_{i=1}^2 \left(\sum_{T \in \mathcal{T}_i} \left(h_i^{2r+1} \|\partial_{x_i}^{r+1} u\|_{0,T}^2 + \frac{h_{i^*}^{2r+2}}{h_i} \|\partial_{x_{i^*}}^{r+1} u\|_{0,T}^2 \right. \right. \\ & \left. \left. + h_i h_{i^*}^{2r} \|\partial_{x_i} \partial_{x_{i^*}}^r u\|_{0,T}^2 + h_i^{2r-1} h_{i^*}^2 \|\partial_{x_i}^r \partial_{x_{i^*}} u\|_{0,T}^2 \right) \right)^{1/2}, \end{aligned}$$

where $\bar{\Phi}(r, k) := \max\{\Phi_{12}(k, r), \frac{5}{2}\Phi_2(k, r-1)\}$. The constant C depends only on the constant in the trace inequality (3.7) and on the constant in Lemma 3.2.

Proof. We consider the decomposition

$$u - u_{\text{RFB}} = (u - Pu) + (Pu - u_{\text{RFB}}),$$

where P is the approximation operator described in the previous section. By employing the coercivity of \mathcal{L} and the Galerkin orthogonality property, on recalling that $Pu \in V_{\text{RFB}}$, we have that

$$\begin{aligned} \varepsilon|u - u_{\text{RFB}}|_{1,\Omega}^2 &\leq \mathcal{L}(u - u_{\text{RFB}}, u - u_{\text{RFB}}) \\ &= \mathcal{L}(u - u_{\text{RFB}}, u - Pu). \end{aligned}$$

Thus, on applying the Cauchy–Schwarz inequality to $\mathcal{L}(u - u_{\text{RFB}}, u - Pu)$ after rewriting it explicitly using the definition of the bilinear form (2.3), we get

$$\begin{aligned} \varepsilon|u - u_{\text{RFB}}|_{1,\Omega}^2 &\leq \sum_{T \in \mathcal{T}_h} \left(\varepsilon \int_T \nabla(u - u_{\text{RFB}}) \cdot \nabla(u - P_T u) \, d\mathbf{x} \right. \\ &\quad \left. + \int_T \mathbf{a} \cdot \nabla(u - u_{\text{RFB}})(u - P_T u) \, d\mathbf{x} \right) \\ &\leq \sum_{T \in \mathcal{T}_h} \left(\varepsilon^{1/2}|u - u_{\text{RFB}}|_{1,T} \right) \left(\varepsilon^{1/2}|u - P_T u|_{1,T} + \varepsilon^{-1/2}\|u - P_T u\|_{0,T} \right) \\ &\leq \varepsilon^{1/2}|u - u_{\text{RFB}}|_{1,\Omega} \left(\sum_{T \in \mathcal{T}_h} \left(\varepsilon^{1/2}|u - P_T u|_{1,T} + \varepsilon^{-1/2}\|u - P_T u\|_{0,T} \right)^2 \right)^{1/2}. \end{aligned}$$

Next, we split the sum on the right-hand side between the subpartitions \mathcal{T}_1 and \mathcal{T}_2 to obtain

$$\varepsilon^{1/2}|u - u_{\text{RFB}}|_{1,\Omega} \leq C \sum_{i=1,2} \left(\sum_{T \in \mathcal{T}_i} \mathcal{E}_T^P(u) \right)^{1/2},$$

with $\mathcal{E}_T^P(u)$ as in (3.10). The required bound now follows from (3.13). \square

Remark. When the problem (2.1) is strongly convection-dominated, the solution is highly anisotropic locally. For this reason it is crucial that the error is bounded by appropriately weighted norms of directional derivatives of the solution, as in our error bound (3.14). We also observe that, if the partition is shape-regular, our error bound collapses to the isotropic error estimate (2.12).

We conclude the section with a remark on the extension of the above bound to the case when, in addition to diffusion and convection terms, the equation also contains a reaction term. Suppose therefore that $-\varepsilon\Delta u + \mathbf{a} \cdot \nabla u + cu = f$ in Ω , subject to $u = 0$ on $\partial\Omega$, with $2c - \text{div}(\mathbf{a}) \leq -2c_0$ in Ω , where c_0 is a positive constant. Arguing similarly as in the proof above, we then obtain

$$\begin{aligned}
 & \varepsilon |u - u_{\text{RFB}}|_{1,\Omega}^2 + c_0 \|u - u_{\text{RFB}}\|_{0,\Omega}^2 \\
 & \leq \varepsilon^{1/2} |u - u_{\text{RFB}}|_{1,\Omega} \left(\sum_{T \in \mathcal{T}_h} \left(\varepsilon^{1/2} |u - P_T u|_{1,T} + \varepsilon^{-1/2} \|u - P_T u\|_{0,T} \right)^2 \right)^{1/2} \\
 & \quad + \|c\|_{L^\infty(\Omega)} \|u - u_{\text{RFB}}\|_{0,\Omega} \left(\sum_{T \in \mathcal{T}_h} \|u - P_T u\|_{0,T}^2 \right)^{1/2} \\
 & \leq (\varepsilon |u - u_{\text{RFB}}|_{1,\Omega}^2 + c_0 \|u - u_{\text{RFB}}\|_{0,\Omega}^2)^{1/2} \\
 & \quad \times \left(\sum_{T \in \mathcal{T}_h} \left(\varepsilon^{1/2} |u - P_T u|_{1,T} + \varepsilon^{-1/2} \|u - P_T u\|_{0,T} \right)^2 + \frac{\|c\|_{L^\infty(\Omega)}^2}{c_0} \|u - P_T u\|_{0,T}^2 \right)^{1/2}.
 \end{aligned}$$

The rest of the argument, based on bounding the second factor on the right-hand side in the final inequality, proceeds as in the proof of Theorem 3.8.

4. Affine partitions. We now discuss the case of partitions \mathcal{T}_h consisting of affine-equivalent (triangular or quadrilateral) elements. As before, our assumptions on the partition are conformity and that (2.4) holds.

The following a priori error analysis is based on Lemma 3.2 and on the technique introduced by Formaggia and Perotto [14] (see also the references therein and Micheletti, Perotto, and Picasso [25]) to prove anisotropic error estimates for the interpolation error. More precisely, we will employ suitable scaling properties derived in [14] in terms of certain characteristic quantities of the affine transformation F_T . A limitation of the approach is that only an a priori error bound in terms of the H^2 -seminorm can be obtained, so this analysis applies only in the case when $k = 1$. An extension of the bounds presented here to the case when $k \geq 1$ can be carried out using the techniques developed in section 2.2 of the paper of Huang [20].

Let $F_T(\hat{x}) = M\hat{x} + \mathbf{t}$ (we omit the dependence of M and \mathbf{t} on T to simplify the notation). As the matrix M is invertible, it admits a unique *polar decomposition* $M = BZ$, where B is symmetric and positive definite and Z is orthonormal.

Further, B is factorized as $B = R^T \Lambda R$, where Λ is diagonal with positive decreasing entries (the eigenvalues of B) and R is orthonormal (with rows which are the eigenvectors of B). Hence,

$$\Lambda = \begin{bmatrix} \lambda_1 & 0 \\ 0 & \lambda_2 \end{bmatrix}, \quad R = \begin{bmatrix} \mathbf{r}_1^T \\ \mathbf{r}_2^T \end{bmatrix},$$

where $\lambda_1 \geq \lambda_2$ and $\mathbf{r}_1, \mathbf{r}_2$ are the eigenvalues and eigenvectors of B , respectively. The above decomposition corresponds to the singular value decomposition $M = R^T \Lambda Q$, with $Q = RZ$: The reference element \hat{T} is rotated using Q , stretched by Λ , and then rotated again by R^T . The translation \mathbf{t} finally gives the correct location of T . The eigenvalues λ_1 and λ_2 of Λ thus give the element dimensions in a rotated orthogonal frame and hence are used to replace h_1 and h_2 from the previous section as the characteristic dimensions of the element T .

With this new notation, we get the following scaling rules, which are the counterparts of (3.1) and (3.2):

$$(4.1) \quad \|v\|_{0,T}^2 = \lambda_1 \lambda_2 \|\hat{v}\|_{0,\hat{T}}^2,$$

$$(4.2) \quad |v|_{1,T}^2 \leq \frac{\lambda_1}{\lambda_2} |\hat{v}|_{1,\hat{T}}^2.$$

The equality (4.1) is elementary, while (4.2) is proved in [14] as Lemma 2.2.

To scale back from the reference element we shall use the following identity which is Lemma 2.2 in [25] (see also the proof of Lemmas 2.1 and 2.2 in [14]):

$$(4.3) \quad |\hat{v}|_{2,\hat{T}}^2 = \frac{\lambda_1^3}{\lambda_2} L_{11}v + \frac{\lambda_2^3}{\lambda_1} L_{22}v + 2\lambda_1\lambda_2 L_{12}v,$$

where

$$(4.4) \quad L_{ij}v := \int_T (\mathbf{r}_i^T H(v) \mathbf{r}_j)^2 \, d\mathbf{x}, \quad \text{with } i, j = 1, 2,$$

and $H(v)$ is the Hessian matrix associated with the function v ; that is,

$$H(v) := \begin{bmatrix} \frac{\partial^2 v}{\partial x_1^2} & \frac{\partial^2 v}{\partial x_1 \partial x_2} \\ \frac{\partial^2 v}{\partial x_1 \partial x_2} & \frac{\partial^2 v}{\partial x_2^2} \end{bmatrix}.$$

THEOREM 4.1. *Let $u \in V$ be the solution of (2.2) and $u_{\text{RFB}} \in V_{\text{RFB}}$ the RFB solution defined by (2.8). Consider a conforming affine-equivalent partition \mathcal{T}_h assuming that there exists a constant $c \in (0, 1]$ such that, for every $T \in \mathcal{T}_h$, $\varepsilon \leq c\lambda_2$, where $\lambda_1 \geq \lambda_2$ are the characteristic dimensions of T defined above.*

If $u \in H_0^1(\Omega) \cap H^2(\Omega)$, then there exists a positive constant C , independent of the mesh dimensions and of ε , such that

$$(4.5) \quad \varepsilon^{1/2} |u - u_{\text{RFB}}|_{1,\Omega} \leq C \left(\sum_{T \in \mathcal{T}_h} \left(\frac{\lambda_1^4}{\lambda_2} L_{11}u + \lambda_2^3 L_{22}u + 2\lambda_1^2 \lambda_2 L_{12}u \right) \right)^{1/2},$$

where the terms L_{ij} , $i, j = 1, 2$, are defined elementwise as in (4.4) in terms of the Hessian of the function u .

Proof. Let $T \in \mathcal{T}_h$. As in the previous section, we need to bound the quantity given by (3.10); that is,

$$\mathcal{E}_T^I(v) = \varepsilon |v - P_T v|_{1,T}^2 + \varepsilon^{-1} \|v - P_T v\|_{0,T}^2,$$

where $v \in H^1(T)$. As before, we start by scaling $\mathcal{E}_T^I(v)$ to the reference element \hat{T} . Using (4.1) and (4.2) we get

$$(4.6) \quad \begin{aligned} \mathcal{E}_T^I(v) &\leq \varepsilon \frac{\lambda_1}{\lambda_2} |\hat{v} - P_{\hat{T}} \hat{v}|_{1,\hat{T}}^2 + \varepsilon^{-1} \lambda_1 \lambda_2 \|\hat{v} - P_{\hat{T}} \hat{v}\|_{0,\hat{T}}^2 \\ &= \lambda_1 \left(\frac{\varepsilon}{\lambda_2} |\hat{v} - P_{\hat{T}} \hat{v}|_{1,\hat{T}}^2 + \left(\frac{\varepsilon}{\lambda_2} \right)^{-1} \|\hat{v} - P_{\hat{T}} \hat{v}\|_{0,\hat{T}}^2 \right). \end{aligned}$$

We then apply Lemma 3.2, this time with $\hat{w}_0 = (\hat{v} - \hat{\pi}_1 \hat{v})|_{\partial \hat{T}}$, where $\hat{\pi}_1$ is the standard linear Lagrange interpolant (that is, $\hat{\pi}_k$, with $k = 1$) defined on the reference triangle \hat{T} , and with $t = \varepsilon/\lambda_2$. In this way we get

$$\mathcal{E}_T^I(v) \leq C \left(\varepsilon \frac{\lambda_1}{\lambda_2} |\hat{v} - \hat{\pi}_1 \hat{v}|_{1/2,\partial \hat{T}}^2 + \lambda_1 \|\hat{v} - \hat{\pi}_1 \hat{v}\|_{0,\partial \hat{T}}^2 \right).$$

Instead of scaling back to the boundary of the element T as was done previously, we now proceed by applying the trace inequality (3.4) and the standard Lagrange

interpolation error bounds on \widehat{T} (see Ciarlet [13]). Since $\lambda_2 \leq \lambda_1$ and $\varepsilon \leq c\lambda_2$, with $c \in (0, 1]$, we get

$$\begin{aligned}
 \mathcal{E}_T^I(v) &\leq C \left(\varepsilon \frac{\lambda_1}{\lambda_2} + \lambda_1 \right) \|\hat{v} - \hat{\pi}_1 \hat{v}\|_{1,\widehat{T}}^2 \\
 &\leq C \lambda_1 |\hat{v}|_{2,\widehat{T}}^2 \\
 (4.7) \quad &\leq C \left(\frac{\lambda_1^4}{\lambda_2} L_{11} v + \lambda_2^3 L_{22} v + 2\lambda_1^2 \lambda_2 L_{12} v \right),
 \end{aligned}$$

the last bound being a consequence of (4.3). The desired error bound now follows by repeating the steps in the proof of Theorem 3.8. \square

If the partition \mathcal{T}_h is axiparallel, then $\lambda_i = h_i/c_i$, with h_i and c_i , $i = 1, 2$, being the dimensions along the coordinate axes of T and \widehat{T} , respectively. In this case Theorem 4.1 collapses to the a priori error bound (3.14), with $r = 1$.

5. Numerical examples. As discussed in section 1, a fully discrete RFB method is obtained after approximating the bubble space. In the following experiment, the local bubble problem on each element is solved using the standard Galerkin finite element method (FEM) on an 8×8 Shishkin partition. This is a piecewise uniform mesh with half of the nodes in each coordinate direction lying in the boundary-layer region of the element; see [24] and references therein. This choice abundantly ensures that the subgrid discretization error is of higher order than the RFB error controlled by our error analysis. In fact, in the case of P_1 shape-regular finite elements, it has been proved by Brezzi and Marini [8] that a subgrid consisting of a single internal node placed inside the boundary layer of the bubble problem is sufficient; see also [4]. This is the fully discrete method that we suggest for practical implementations.

Another possibility, exploited in further experiments presented later on, is to discretize the convection field with piecewise constants and then approximate the solution of each local bubble problem by the solution of the corresponding reduced (hyperbolic) elemental problem [9]. This procedure is computationally inexpensive, as it amounts to the calculation of the volume of a pyramid on each element. Moreover, when the problem is convection-dominated, such an approximation does not compromise the accuracy of the method (a choice that is optimal in all regimes is the link-cutting bubble proposed in [4] for one-dimensional problems). Indeed, the discretization of the bubble functions need not be particularly accurate as long as the elemental average

$$\frac{\int_T b_T \, d\mathbf{x}}{|T|}$$

of the bubble b_T has been sufficiently accurately approximated; the reason, as is shown later on in this paper (see also [5]), is that only the elemental averages of the bubbles enter into the fully discrete method. The behavior of the above term on shape-regular partitions, as a function of the mesh Péclet number $\mathbf{Pe}_T = h_T |\mathbf{a}|/\varepsilon$, is analyzed in [5], where it is also shown that the average of the solution of the reduced bubble problem behaves similarly in the convection-dominated regime to the average of the exact bubble b_T . Lemma 6.1 below extends the analysis from [5] to anisotropic partitions, thus suggesting that this simple recipe for full discretization is still viable on anisotropic partitions.

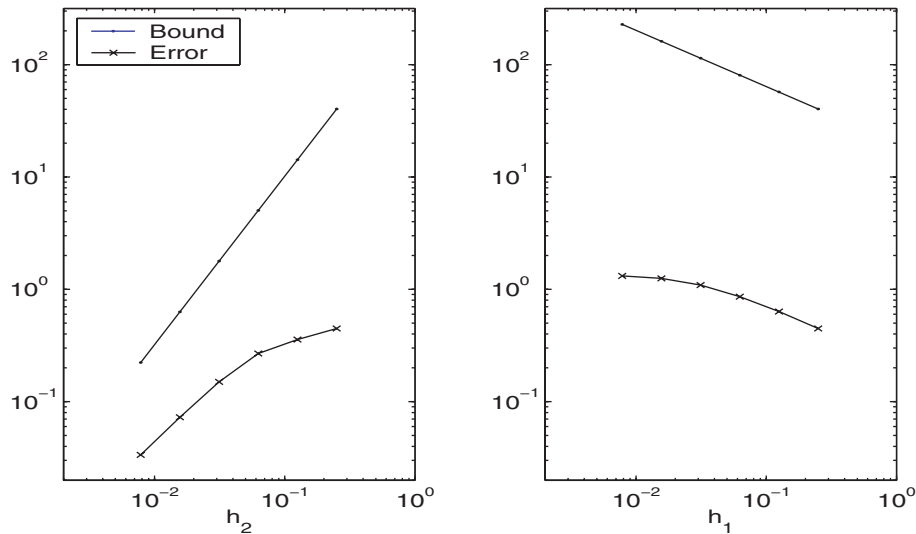


FIG. 5.1. $\varepsilon^{1/2}$ -weighted H^1 -seminorm error and error bound under (the correct) h_2 -refinement (left) and (the incorrect) h_1 -refinement (right); $\varepsilon = 10^{-2}$. In both cases, we start from the 4×4 uniform square mesh.

We consider the following simple boundary-value problem

$$(5.1) \quad \begin{cases} -\varepsilon \Delta u + u_{x_2} = 0 & \text{in } \Omega = (0, 1)^2, \\ u(x_1, 0) = 0; \quad u(x_1, 1) = 1, & x_1 \in [0, 1], \\ u_{x_1} = 0 & \text{on } \Gamma_N = (\{0\} \times (0, 1)) \cup (\{1\} \times (0, 1)), \end{cases}$$

whose solution is given by

$$u(x_1, x_2) = \frac{e^{x_2/\varepsilon} - 1}{e^{1/\varepsilon} - 1}.$$

We consider discretizations of this problem with respect to axiparallel uniform rectangular grids of dimensions h_1 and h_2 in the respective coordinate directions. For this problem the error bound (3.14) reduces to

$$\varepsilon^{1/2} |u - u_{\text{RFB}}|_{1,\Omega} \leq C \begin{cases} h_2^3 \|\partial_{x_2}^2 u\|_{0,\Omega}^2 & \text{if } h_2 \leq h_1, \\ \frac{h_2^4}{h_1} \|\partial_{x_2}^2 u\|_{0,\Omega}^2 & \text{if } h_2 > h_1. \end{cases}$$

We verify the validity of the bound by performing the following tests. Starting from the uniform 4×4 mesh, we either

- fix h_1 while halving h_2 (*correct refinement*) or
- fix h_2 while halving h_1 (*incorrect refinement*).

The relevant energy norm errors and error bounds are shown in the log-log plot in Figure 5.1 (left-hand panel) for $\varepsilon = 10^{-2}$.

Performing the correct refinement is, of course, not too different from solving the related sequence of one-dimensional problems. The similarity of the numerical solution of the two-dimensional problem to the numerical solution of the related one-dimensional problem is lost when the incorrect refinement is performed (notice that

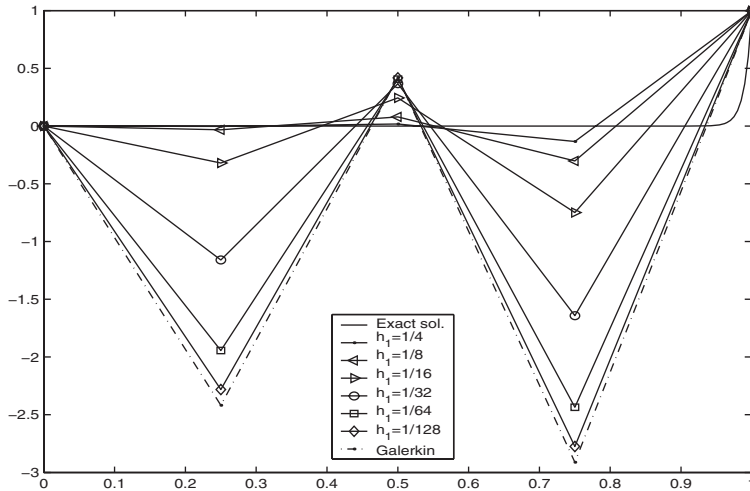


FIG. 5.2. Profile of the solution along $x_1 = 1/2$ under h_1 -refinement (as in the right-hand panel in Figure 5.1), while $h_2 = 1/4$. The lowest profile represents the piecewise \mathcal{Q}_1 standard Galerkin FEM solution computed on a uniform 4×4 mesh. The exact solution is also plotted for comparison.

this does not happen when applying the standard Galerkin method with linear elements). As predicted by the error bound, the accuracy of the solution actually deteriorates under the incorrect refinement; see the log-log plot in Figure 5.1 (right-hand panel). This is due to the peculiar definition of the RFB finite element space. Mesh refinement corresponds to a relative impoverishment of the bubble subspace and an enrichment of the piecewise polynomial subspace. If the latter enrichment, as is the case with our incorrect refinement, is ineffective, then the overall approximation properties of V_{RFB} will be worse than on a coarser mesh. The detailed error analysis of the RFB method on shape-regular partitions presented in our recent work [12] aims to clarify the approximation properties of the method in the preasymptotic regime when $\varepsilon \leq ch$. In particular, in [12], we relate the phenomenon just observed to the inadequacy of V_h^k to capture the exponential behavior of the solution along element edges contained in the boundary layer.

In the limit of $h_1 \rightarrow 0$, the solution becomes constant along x_1 . That is, it tends to the piecewise \mathcal{Q}_1 standard Galerkin solution, which is unaffected by the reduction of h_1 ; see Figure 5.2. Asymptotically, in the case of the incorrect refinement (with $h_1 \rightarrow 0$), the error is of order $O(1)$ (cf. Figure 5.1 (right)). In other words, since the bubble part of the solution is forced to tend to zero as $h_1 \rightarrow 0$, its stabilizing effect is diminished until, in the limit, it vanishes and the RFB method collapses to the standard Galerkin FEM. This fact shows that the stabilization properties of stabilized FEMs are affected by the anisotropy of the partition.

The use of anisotropic partitions for the solution of highly convection-dominated problems can become mandatory if resolution of thin layers in the solution is paramount. Let us consider, for example, the boundary-value problem

$$(5.2) \quad \begin{cases} -\varepsilon \Delta u + (2, 1)^T \cdot \nabla u = 0 & \text{in } \Omega = (0, 1)^2, \\ u(x_1, 0) = u(1, x_2) = 0, & x_1, x_2 \in (0, 1), \\ u(x_1, 1) = u(0, x_2) = 1, & x_1, x_2 \in [0, 1]. \end{cases}$$

The solution of (5.2) exhibits an internal layer emanating from the origin of the coor-

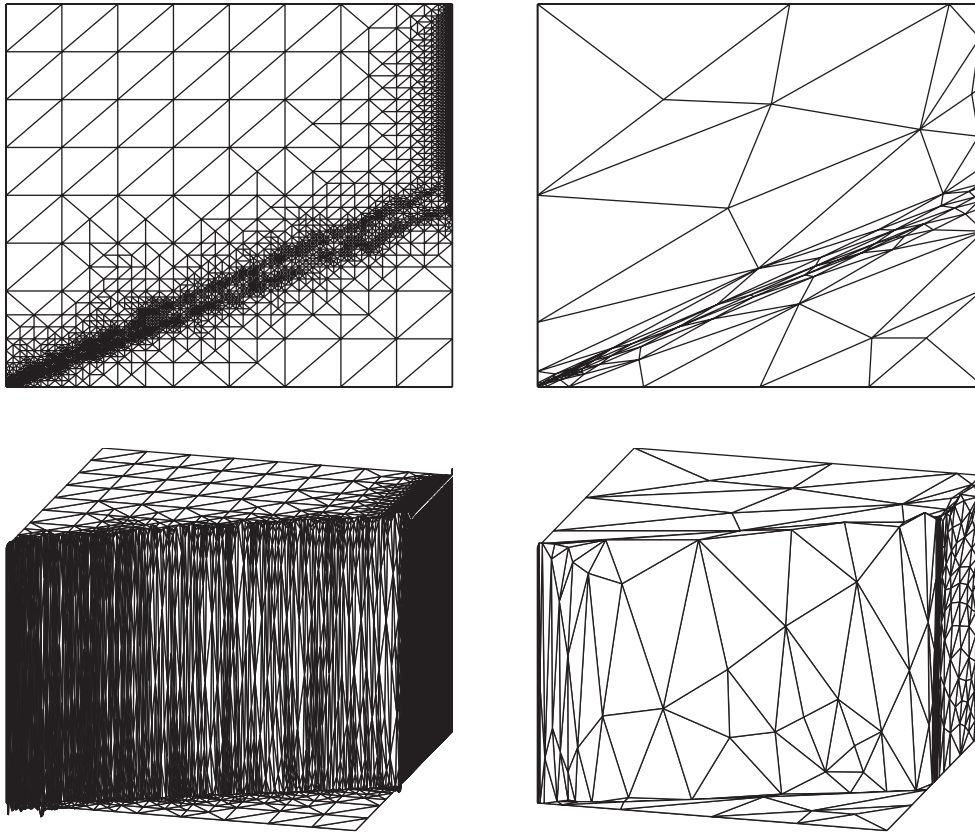


FIG. 5.3. The solution of (5.2) with $\varepsilon = 10^{-4}$ on ad hoc-refined triangulations. Left: Shape-regular mesh (23256 elements, 12693 nodes) and the corresponding solution. Right: Anisotropic mesh (478 elements, 263 nodes) and the corresponding solution.

dinate system and a boundary layer situated along $x_1 = 1$. The RFB approximation of (5.2) is shown in Figure 5.3. The bubble solution is approximated by the solution of the related reduced (hyperbolic) elemental problem [9]. We compute the RFB solution using, respectively, a shape-regular triangulation (left-hand panels in the figure) and an anisotropic triangulation (right-hand panels in the figure). The anisotropic triangulation has been generated by Picasso [26], by applying a ZZ-type error indicator for the gradient error to the classical stabilized Galerkin least-squares (GLS) method, until the stopping criterion ZZ-indicator $\leq 1/4$ was satisfied in all elements. The triangulation was then used to compute the RFB solution shown in the bottom right-hand panel of Figure 5.3. The computation on the shape-regular triangulation was performed by applying the residual-based L^2 -error indicator proposed in [10] for the RFB method. For the sake of consistency, the adaptation was stopped when the error indicator fell below $1/4$ in all elements. The RFB solution computed on the anisotropic triangulation is clearly superior, as the triangulation consists of only 263 nodes instead of the 12693 nodes, with comparable accuracy, in the case of the shape-regular partition.

6. Tuning of the SD parameter. The RFB method is closely related to classical stabilized finite element methods (streamline upwind Petrov–Galerkin (SUPG),

GLS, etc.). For instance, in the case of piecewise constant coefficients and linear finite elements, RFB is equivalent to SUPG and GLS (the latter methods coincide in this case with what Johnson, Nävert, and Pitkäranta [22] refer to as the *streamline-diffusion finite element method* (SDFEM)). Here we exploit this identification to obtain a theoretically justified value of the user-selected stabilization parameter in stabilized finite element methods.

We consider the RFB method (2.8), assuming that \mathcal{T}_h consists of triangles, and fix $k = 1$. In this case, $V_{\text{RFB}} = V_h^1 \oplus B_h$, where V_h^1 is the space of linear finite elements.

Let us also assume that \mathbf{a} and f are constant on every element of \mathcal{T}_h . Then the right-hand side of (2.11) is constant, and the bubble part of the RFB solution is given locally on T by $u_b|_T = (f - Lu_h)|_T b_T$, where $b_T \in H_0^1(T)$ satisfies

$$(6.1) \quad -\varepsilon \Delta b_T + \mathbf{a} \cdot \nabla b_T = 1.$$

Substituting u_b into (2.9) it follows that $u_h \in V_h^1$ is the solution of

$$(6.2) \quad \mathcal{L}(u_h, v_h) + \sum_{T \in \mathcal{T}_h} \frac{\int_T b_T \, d\mathbf{x}}{|T|} (\mathbf{a} \cdot \nabla u_h - f, \mathbf{a} \cdot \nabla v_h)_T = (f, v_h) \quad \forall v_h \in V_h^1.$$

The formulation (6.2) coincides with the SDFEM with the particular choice of the SD parameter given by

$$(6.3) \quad \tau_b := \frac{\int_T b_T \, d\mathbf{x}}{|T|}.$$

Thus, as anticipated, the RFB method and the SDFEM are, in this case, equivalent. This well-known fact was first observed by Brezzi and Russo [9].

A numerical method is obtained from the RFB formulation by considering (6.2) where the quantity τ_b has been suitably approximated (examples are given in [9, 15, 6, 8, 4, 30, 11]). As discussed in [5] in the case of shape-regular triangulations, the crucial property is that the approximated value of τ_b scales as τ_b with respect to the mesh size and the coefficients ε and \mathbf{b} .

Specifically, let h_a indicate the length of the longest segment parallel to \mathbf{a} contained in T . On shape-regular partitions, i.e., assuming that the minimal angle of T is bounded below by a fixed positive constant, we know from [5] that

$$(6.4) \quad C \frac{h_T}{|\mathbf{a}|} \min \left\{ \frac{h|\mathbf{a}|}{\varepsilon}, 1 \right\} \leq \tau_b \leq \frac{h_a}{|\mathbf{a}|}.$$

In practice, $\tau_b \sim \frac{h_T}{|\mathbf{a}|} \min \left\{ \frac{h|\mathbf{a}|}{\varepsilon}, 1 \right\}$, which is qualitatively the value of the SD parameter suggested by the a priori error analysis of the SDFEM (see, e.g., [28]).

The situation is less clear when considering anisotropic elements. Attempts have been made to derive the optimal behavior of the SD parameter through a priori analysis; see, e.g., [3, 23, 25]. The outcome of the investigations in these papers is that the stabilization parameter should depend on the smaller dimension of the element.

For instance, assume that T is a right-angled triangle of dimensions h_1, h_2 , and let $h_{\min} = \min\{h_1, h_2\}$. Then, according to [25], we should choose the SD parameter as

$$(6.5) \quad \tau_{\text{sd}} := C \frac{h_{\min}}{2|\mathbf{a}|} \min \left\{ \frac{h_{\min}|\mathbf{a}|}{6\varepsilon}, 1 \right\}.$$

This choice seems less favorable when the mesh is not aligned with the solution (as in the incorrect refinement in our example above). We notice that in this case the a priori analysis does not predict convergence anyway.

By appropriately modifying the argument employed in [5] to derive (6.4), we shall now obtain a new lower bound for τ_b that takes the two characteristic dimensions of T into account. This result is then used to provide a new rule for selecting the SD parameter.

LEMMA 6.1. *Suppose that T is a right-angled triangle, oriented along the coordinate axes, of dimensions h_1, h_2 ; then the quantity τ_b given by (6.3), where b_T solves (6.1), satisfies*

$$(6.6) \quad C \frac{h_a}{|\mathbf{a}|} \min \{\text{Pe}_T, 1\} \leq \tau_b \leq \frac{h_a}{|\mathbf{a}|},$$

with $C = 1/45$ and with the following definition of the element Péclet number:

$$(6.7) \quad \text{Pe}_T := h_{\min}^2 \frac{|\mathbf{a}|}{8\varepsilon h_a}.$$

Proof. The upper bound is already given in (6.4). Assume that $h_2 < h_1$, so that $h_{\min} = h_2$. To prove the lower bound, we map T into the right-angled triangle \hat{T} with its two orthogonal edges of length $h_a h_1/h_2^2$ and h_a/h_2 aligned with the positive semiaxes of the coordinate system (\hat{x}_1, \hat{x}_2) . The image \hat{b} of $b_T \in H_0^1(T)$ satisfies

$$-\varepsilon \frac{h_a}{h_2^2} \Delta \hat{b} + \mathbf{a} \cdot \nabla \hat{b} = \frac{h_2^2}{h_a} \quad \text{in } \hat{T},$$

and we have

$$(6.8) \quad \tau_b = \frac{2h_2^3}{h_1 h_a^2} \int_{\hat{T}} \hat{b} \, d\hat{\mathbf{x}}.$$

To bound the integral in (6.8) we proceed as in [5]. We let $\hat{\lambda}_1, \hat{\lambda}_2$, and $\hat{\lambda}_3$ be the barycentric coordinates on \hat{T} , define $\hat{b}_3 := \hat{\lambda}_1 \hat{\lambda}_2 \hat{\lambda}_3$, and note that

$$(6.9) \quad \int_{\hat{T}} \hat{b}_3 \, d\hat{\mathbf{x}} = \frac{h_a^2 h_1}{120 h_2^3}.$$

Since $h_2 < h_1$, we have

$$(6.10) \quad M_{\Delta} := \frac{1}{8} \max_{\hat{T}} |\Delta \hat{b}_3| = \frac{1}{4} \frac{h_2^5}{h_a^3 h_1} \max_{\hat{T}} \left(\frac{\hat{x}_1}{h_2} + \frac{\hat{x}_2}{h_1} \right) = \frac{1}{4} \frac{h_2^2}{h_a^2},$$

the maximum being attained at the vertex $(h_a h_1/h_2^2, 0)$, and

$$\begin{aligned}
 M_g &:= \frac{1}{|\mathbf{a}|} \max_{\hat{T}} |\mathbf{a} \cdot \nabla \hat{b}_3| \\
 &= \frac{h_2^3}{|\mathbf{a}| h_a^2 h_1} \max_{\hat{T}} \left| a_1 \left(\hat{x}_2 - 2 \frac{h_2^2}{h_a h_1} \hat{x}_1 \hat{x}_2 - \frac{h_2}{h_a} \hat{x}_2^2 \right) \right. \\
 &\quad \left. + a_2 \left(\hat{x}_1 - \frac{h_2^2}{h_a h_1} \hat{x}_1^2 - 2 \frac{h_2}{h_a} \hat{x}_1 \hat{x}_2 \right) \right| \\
 &\leq \frac{h_2^3}{|\mathbf{a}| h_a^2 h_1} \left(|a_1| \max_{\hat{T}} \left| \hat{x}_2 - 2 \frac{h_2^2}{h_a h_1} \hat{x}_1 \hat{x}_2 - \frac{h_2}{h_a} \hat{x}_2^2 \right| \right. \\
 &\quad \left. + |a_2| \max_{\hat{T}} \left| \hat{x}_1 - \frac{h_2^2}{h_a h_1} \hat{x}_1^2 - 2 \frac{h_2}{h_a} \hat{x}_1 \hat{x}_2 \right| \right) \\
 &= \frac{h_2^3}{|\mathbf{a}| h_a^2 h_1} \left(|a_1| \frac{h_a}{4 h_2} + |a_2| \frac{h_a h_1}{4 h_2^2} \right) \\
 (6.11) \quad &= \frac{1}{4 |\mathbf{a}|} \left(|a_1| \frac{h_2^2}{h_a h_1} + |a_2| \frac{h_2}{h_a} \right),
 \end{aligned}$$

both maxima being attained at the midpoint of the hypotenuse. We note that if $\text{sign}(a_1) = \text{sign}(a_2)$, the above bound reduces to an equality.

We now define

$$\gamma := \frac{1}{M_\Delta + M_g} \min \left\{ \frac{h_2^2}{8 \varepsilon h_a}, \frac{1}{|\mathbf{a}|} \right\}, \quad \hat{w} := \gamma \hat{b}_3, \quad \hat{v} := \frac{h_a}{h_2^2} \hat{b},$$

and introduce the differential operator

$$\hat{L}\varphi := -\varepsilon \frac{h_a}{h_2^2} \Delta \varphi + \mathbf{a} \cdot \nabla \varphi.$$

By the definition of γ , \hat{w} , M_Δ , and M_g , we have

$$|\hat{L}\hat{w}| \leq \gamma \left(\varepsilon \frac{h_a}{h_2^2} M_\Delta + |\mathbf{a}| M_g \right) \leq 1.$$

Thus, by the definition of \hat{v} , we have

$$\hat{L}(\hat{v} - \hat{w}) = \frac{h_a}{h_2^2} \hat{L}\hat{b} - \hat{L}\hat{w} = 1 - \hat{L}\hat{w} \geq 0,$$

and, since both \hat{v} and \hat{w} vanish on $\partial\hat{T}$, using the maximum principle, we conclude that $\hat{v} \geq \hat{w}$ in \hat{T} . We are now ready to bound τ_b . Recalling (6.8) and (6.9), we have

$$\tau_b = \frac{2h_2^5}{h_a^3 h_1} \int_{\hat{T}} \hat{v} \, d\hat{\mathbf{x}} \geq \frac{2h_2^5}{h_a^3 h_1} \gamma \int_{\hat{T}} \hat{b}_3 \, d\hat{\mathbf{x}} = \frac{h_2^2}{60 h_a} \gamma.$$

Further, using the definition of γ , and inserting (6.10) and (6.11), we have

$$\tau_b \geq \frac{1}{15 \left(\frac{|\mathbf{a}|}{h_a} + \frac{|a_1|}{h_1} + \frac{|a_2|}{h_2} \right)} \min \left\{ \frac{|\mathbf{a}| h_2^2}{8 \varepsilon h_a}, 1 \right\}.$$

We distinguish between the following two cases.

- If $\text{sign}(a_1) = \text{sign}(a_2)$, then h_a is the length of the line segment oriented with \mathbf{a} which joins the hypotenuse of T with the opposite vertex. Thus,

$$h_a = \sqrt{\frac{h_2^2}{\left(\frac{a_2}{a_1} + \frac{h_2}{h_1}\right)^2} \left(1 + \frac{a_2^2}{a_1^2}\right)} = \frac{|\mathbf{a}|}{\frac{|a_1|}{h_1} + \frac{|a_2|}{h_2}}.$$

It follows that $|a_1|/h_1 + |a_2|/h_2 = |\mathbf{a}|/h_a$.

- If $\text{sign}(a_1) \neq \text{sign}(a_2)$ and $|a_2|/h_2 > |a_1|/h_1$, then h_a is the length of the line segment oriented with \mathbf{a} which joins the edge of T parallel to the x_1 -axis with the opposite vertex. Thus,

$$h_a = \sqrt{h_2^2 + \frac{a_1^2}{a_2^2} h_2^2} = \frac{h_2 |\mathbf{a}|}{|a_2|},$$

and so $|a_2|/h_2 = |\mathbf{a}|/h_a$. Similarly, if $|a_2|/h_2 > |a_1|/h_1$, then $|a_1|/h_1 = |\mathbf{a}|/h_a$.

It follows that

$$\frac{|\mathbf{a}|}{h_a} + \frac{|a_1|}{h_1} + \frac{|a_2|}{h_2} \leq C \frac{|\mathbf{a}|}{h_a},$$

with $C = 2$ or 3 , depending on the cases listed above, respectively.

Since the above argument can be repeated in the case $h_1 \leq h_2$ by interchanging the role of h_1 and h_2 , we conclude that the bound (6.6) holds with $C = 1/45$. \square

To verify the bound obtained, we compare the behavior of

$$\tau_a := C \frac{h_a}{|\mathbf{a}|} \min \{\mathbf{P}_{\mathbf{e}_T}, 1\},$$

with that of τ_b with respect to the dimensions of T . We let $h_1 = 1$ while halving h_2 starting from $h_2 = 1$. We do this twice in succession, with $\mathbf{a} = (1, 0)$ and then with $\mathbf{a} = (0, 1)$. The results are shown in Figure 6.1 (τ_b is calculated by solving (6.1) very accurately). The superimposition of the graphs is obtained by renormalizing τ_a (the factor is always around 3) so that its first values coincide with that of τ_b . As we can see in Figure 6.1, τ_a and τ_b are very close to each other.

Figure 6.1 also reports the results obtained with the choice τ_{sd} given by (6.5), which was proposed as a SD parameter in [3, 23, 25]. We notice that the two choices τ_a and τ_{sd} have different turning points, particularly when \mathbf{a} is aligned with the longest edge of T . This is due to the fact that our definition of the element Péclet number depends not only on the magnitude of the convective field, but also on its direction. We believe that this should indeed be the case when anisotropic partitions are considered, and hence we propose τ_a as the appropriate SD parameter. The definition of τ_a easily extends to a general element by substituting h_1 and h_2 by the characteristic dimensions λ_1 and λ_2 .

We assess experimentally our new choice of the SD parameter τ_a by comparing its performance with that of τ_{sd} on some model problems. From the discussion above we know that the two choices τ_a and τ_{sd} differ the most when the stretching of the element is aligned with the direction of convection. We must also take into account, though, that the magnitude of the SDFEM stabilization term depends on the alignment of the convection with the gradient of the solution; cf. (6.2); see also section 3 in [20]. We therefore consider two test problems: (5.1), whose solution exhibits a boundary layer,

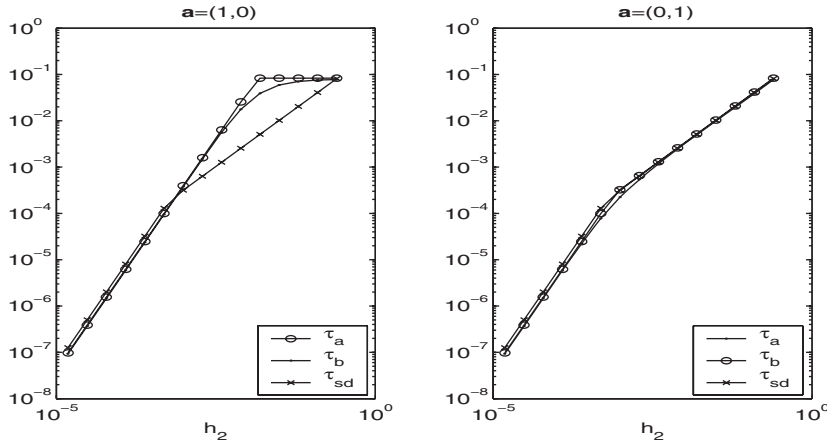


FIG. 6.1. Comparisons of τ_b with τ_a and τ_{sd} on a rectangle of dimensions 1 and h_2 for $\varepsilon = 10^{-4}$.

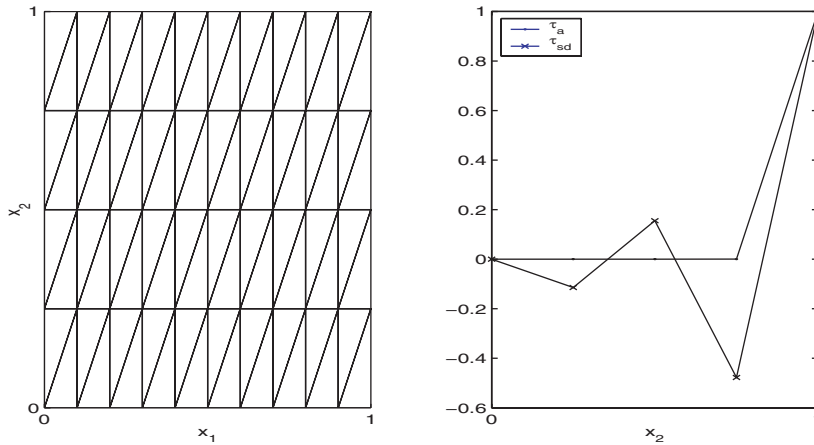


FIG. 6.2. Mesh and SDFEM solution profile along $x_1 = 1/2$ for the model problem (5.1) with $\varepsilon = 10^{-4}$.

and a modification of (5.2) obtained by imposing a Neumann boundary condition on the outflow boundary, so that the solution of the problem contains an internal layer. In all tests we solved the problem on a slightly stretched uniform partition of aspect ratio 4/10.

We start with (5.1). We compare the two different choices of the SD parameter τ_a and τ_{sd} by solving the model problem (5.1) with $\varepsilon = 10^{-4}$ by means of the SDFEM. In both cases, the constant factors C in the definitions of the two parameters are tuned by solving the problem on a uniform partition. We apply the SDFEM on the partition depicted in the left-hand panel of Figure 6.2. The solution profile at $x_1 = 1/2$ is shown in the right-hand panel of Figure 6.2. While the solution obtained using τ_a correctly reproduces the exact solution, the one obtained using τ_{sd} is corrupted by oscillations, indicating that the stabilization parameter τ_{sd} is too small. The difference is due to the fact that, while τ_{sd} always depends on h_{\min} , the parameter τ_a is linked to h_{\max} as long as $\mathbf{Pe}_T > 1$. Eventually, if the mesh is further stretched in the incorrect direction, the

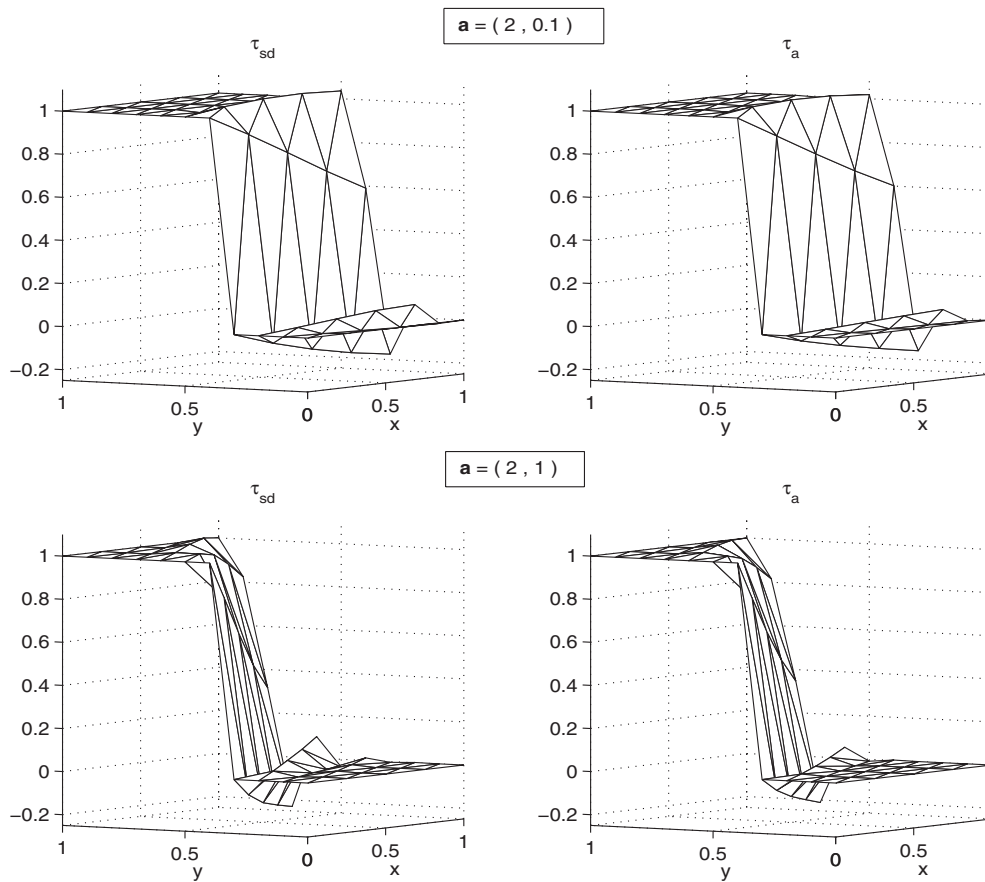


FIG. 6.3. SDFEM solution of the model problem (6.12) with $\varepsilon = 10^{-4}$.

use of τ_a will also lead to maximum-principle-violating oscillations in the numerical solution, but this happens for partitions with significantly higher aspect ratios than for τ_{sd} ; for the present model problem, $\text{Pe}_T > 1$ for $h_{\min} > 2^{5/2}10^{-2} \approx 0.05$, corresponding to an aspect ratio of $1/5$. In conclusion, our choice will guarantee stability for any, *not too unreasonably* designed, partition, such as the one used in the experiment.

We finally consider the following boundary-value problem:

$$(6.12) \quad \begin{cases} -\varepsilon \Delta u + \mathbf{a} \cdot \nabla u = 0 & \text{in } \Omega = (0, 1)^2, \\ u(x_1, 0) = 0; \quad u(x_1, 1) = 1, & x_1 \in (0, 1), \\ u(0, x_2) = \chi_{[1/3, 1]}(x_2); \quad \frac{\partial u}{\partial x_1}(1, x_2) = 0, & x_2 \in [0, 1], \end{cases}$$

which exhibits an internal layer emanating from the boundary-value discontinuity in $(0, 1/3)$ in the direction of \mathbf{a} . We fix the partition to be a uniform 4×10 partition and test the different choices of the SD parameter as functions of the convection direction by setting $\mathbf{a} = (2, 1)$ as in (5.2) and then $\mathbf{a} = (2, 0.1)$, i.e., aligned with the partition. The SDFEM solutions are shown in Figure 6.3. The solutions obtained using τ_a are slightly less oscillatory, particularly in the case $\mathbf{a} = (2, 1)$, where we observe differences in the solutions at the outflow up to a factor of 1.6. This latter fact may seem counterintuitive, as τ_a and τ_{sd} differ the most in the case $\mathbf{a} = (2, 0.1)$

when convection is aligned with the stretching of the partition, but the alignment improves the performance of the method and reduces the need for stabilization.

7. Conclusions. When a convection-diffusion problem is strongly convection-dominated, the solution is often highly anisotropic, exhibiting large gradients in specific directions. In this paper we have developed the a priori error analysis of the RFB method, in the energy norm, on anisotropic partitions. The error is bounded by appropriately weighted norms of directional derivatives of the solution, so as to respect the anisotropic nature of the solution to the problem. The error bound established is an extension of that obtained by Sangalli [29] for shape-regular partitions.

Anisotropy also has to be taken into account in the tuning of the parameters appearing in *streamline-diffusion*-type methods. We have used the stabilizing term derived from the RFB method to redefine the mesh Péclet number and proposed a new choice of the SD parameter which is suitable for use on anisotropic partitions. Our choice improves the choices of the SD parameter presented in previous works based on the a priori analysis of the SD method (cf. [3, 23, 25]).

Acknowledgment. We are grateful to Professor Marco Picasso (Ecole Polytechnique Fédérale de Lausanne) for supplying the anisotropic triangulation that was used to generate the right-hand panels in Figure 5.3.

REFERENCES

- [1] R. A. ADAMS, *Sobolev Spaces*, Pure Appl. Math. (Amst.) 65, Academic Press, New York, 1975.
- [2] T. APEL, *Anisotropic Finite Elements: Local Estimates and Applications*, Adv. Numer. Math., Teubner, Stuttgart, 1999.
- [3] T. APEL AND G. LUBE, *Anisotropic mesh refinement in stabilized Galerkin methods*, Numer. Math., 74 (1996), pp. 261–282.
- [4] F. BREZZI, G. HAUKE, L. D. MARINI, AND G. SANGALLI, *Link-cutting bubbles for the stabilization of convection-diffusion-reaction problems*, Math. Models Methods Appl. Sci., 13 (2003), pp. 445–461.
- [5] F. BREZZI, T. J. R. HUGHES, L. D. MARINI, A. RUSSO, AND E. SÜLI, *A priori error analysis of residual-free bubbles for advection-diffusion problems*, SIAM J. Numer. Anal., 36 (1999), pp. 1933–1948.
- [6] F. BREZZI, D. MARINI, AND A. RUSSO, *Applications of the pseudo residual-free bubbles to the stabilization of convection-diffusion problems*, Comput. Methods Appl. Mech. Engrg., 166 (1998), pp. 51–63.
- [7] F. BREZZI, D. MARINI, AND E. SÜLI, *Residual-free bubbles for advection-diffusion problems: The general error analysis*, Numer. Math., 85 (2000), pp. 31–47.
- [8] F. BREZZI AND L. D. MARINI, *Augmented spaces, two-level methods, and stabilizing subgrids*, Internat. J. Numer. Methods Fluids, 40 (2002), pp. 31–46.
- [9] F. BREZZI AND A. RUSSO, *Choosing bubbles for advection-diffusion problems*, Math. Models Methods Appl. Sci., 4 (1994), pp. 571–587.
- [10] A. CANGIANI AND E. SÜLI, *A-Posteriori Error Estimators and RFB*, Technical report NA-04/22, Computing Laboratory, 2004.
- [11] A. CANGIANI AND E. SÜLI, *Enhanced residual-free bubble method for convection-diffusion problems*, Internat. J. Numer. Methods Fluids, 47 (2005), pp. 1307–1313.
- [12] A. CANGIANI AND E. SÜLI, *Enhanced RFB method*, Numer. Math., 101 (2005), pp. 273–308.
- [13] P. G. CIARLET, *The Finite Element Method for Elliptic Problems*, North-Holland, Amsterdam, 1978.
- [14] L. FORMAGGIA AND S. PEROTTO, *New anisotropic a priori error estimates*, Numer. Math., 89 (2001), pp. 641–667.
- [15] L. P. FRANCA AND A. RUSSO, *Deriving upwinding, mass lumping and selective reduced integration by residual-free bubbles*, Appl. Math. Lett., 9 (1996), pp. 83–88.
- [16] E. GEORGIOULIS, E. HALL, AND P. HOUSTON, *Discontinuous Galerkin methods for advection-diffusion-reaction problems on anisotropically refined meshes*, SIAM J. Sci. Comput., to appear.

- [17] E. H. GEORGIOULIS, *Discontinuous Galerkin Methods on Shape-Regular and Anisotropic Meshes*, D.Phil. thesis, University of Oxford, 2003.
- [18] E. H. GEORGIOULIS AND E. SÜLI, *Optimal error estimates for the hp-version interior penalty discontinuous Galerkin finite element method*, IMA J. Numer. Anal., 25 (2005), pp. 205–220.
- [19] D. GILBARG AND N. S. TRUDINGER, *Elliptic Partial Differential Equations of Second Order*, Classics Math., Springer-Verlag, Berlin, 2001.
- [20] W. HUANG, *Measuring mesh qualities and application to variational mesh adaptation*, SIAM J. Sci. Comput., 26 (2005), pp. 1643–1666.
- [21] W. HUANG, *Mathematical principles of anisotropic mesh adaptation*, Commun. Comput. Phys., 1 (2006), pp. 276–310.
- [22] C. JOHNSON, U. NÄVERT, AND J. PITKÄRANTA, *Finite element methods for linear hyperbolic problems*, Comput. Methods Appl. Mech. Engrg., 45 (1984), pp. 285–312.
- [23] G. KUNERT, *Robust a posteriori error estimation for a singularly perturbed reaction-diffusion equation on anisotropic tetrahedral meshes*, Adv. Comput. Math., 15 (2001), pp. 237–259.
- [24] N. MADDEN AND M. STYNES, *Efficient generation of Shishkin meshes in solving convection-diffusion problems*, Internat. J. Numer. Methods Engrg., 40 (1997), pp. 565–576.
- [25] S. MICHELETTI, S. PEROTTO, AND M. PICASSO, *Stabilized finite elements on anisotropic meshes: A priori error estimates for the advection-diffusion and the Stokes problems*, SIAM J. Numer. Anal., 41 (2003), pp. 1131–1162.
- [26] M. PICASSO, *An anisotropic error indicator based on Zienkiewicz-Zhu error estimator: Application to elliptic and parabolic problems*, SIAM J. Sci. Comput., 24 (2003), pp. 1328–1355.
- [27] U. RISCH, *Convergence analysis of the residual free bubble method for bilinear elements*, SIAM J. Numer. Anal., 39 (2001), pp. 1366–1379.
- [28] H.-G. ROOS, M. STYNES, AND L. TOBISKA, *Numerical Methods for Singularly Perturbed Differential Equations*, Springer-Verlag, Berlin, 1996.
- [29] G. SANGALLI, *Global and local error analysis for the residual-free bubbles method applied to advection-dominated problems*, SIAM J. Numer. Anal., 38 (2000), pp. 1496–1522.
- [30] G. SANGALLI, *A discontinuous residual-free bubble method for advection-diffusion problems*, J. Engrg. Math., 49 (2004), pp. 149–162.
- [31] C. SCHWAB, *p- and hp-Finite Element Methods*, Oxford University Press, New York, 1998.
- [32] H. TRIEBEL, *Interpolation Theory, Function Spaces, Differential Operators*, second ed., Johann Ambrosius Barth, Heidelberg, 1995.